European Radiology

ESR | EUROPEAN SOCIETY OF RADIOLOGY

MAGNETIC RESONANCE

Check for updates

Improved characterization of lenticulostriate arteries using compressed sensing time-of-flight at 7T

Zhe Zhang[1,2] · Qingle Kong[3] · Yingkui Zhang[1,2] · Wanlin Zhu[1,2] · Ning Wei[1,2] · Yuyuan Xu[1,2,4] · Yue Suo[1,2,4] · Xia Meng[1,2,4] · Patrick Liebig[5] · Zihao Zhang[6,7] · Yongjun Wang[1,2,4] · Jing Jing[1,2,4]

Abstract

Objectives To evaluate the feasibility of 0.2-mm isotropic lenticulostriate arteries (LSAs) imaging using compressed sensing time-of-flight (CS TOF) at around 10 min on 7T, and compare the delineation and characterization of LSAs using conventional TOF and CS TOF.

Methods Thirty healthy volunteers were examined with CS TOF and conventional TOF at 7T for around 10 min each. CS TOF was optimized to achieve 0.2-mm isotropic LSA imaging. The numbers of LSA stems and branches were counted and compared on a vascular skeleton. The length and distance were measured and compared on the most prominent branch in each hemisphere. Another patient with intracranial artery stenosis was studied to compare LSA delineation in CS TOF and digital subtraction angiography (DSA).

Results The number of stems visualized with CS TOF was significantly higher than with conventional TOF in both left ($p = 0.002$, ICC $= 0.884$) and right ($p < 0.001$, ICC $= 0.938$) hemispheres. The number of branches visualized by conventional TOF was significantly lower than that by CS TOF in both left ($p < 0.001$, ICC $= 0.893$) and right ($p < 0.001$, ICC $= 0.896$) hemispheres. The lengths were statistically higher in CS TOF than in conventional TOF (left: $p < 0.001$, ICC $= 0.868$; right: $p < 0.001$, ICC $= 0.876$).

Conclusions The high-resolution CS TOF improves the delineation and characterization of LSAs over conventional TOF. High-resolution LSA imaging using CS TOF can be a promising tool for clinical research and applications in patients with neurologic diseases.

Key Points

● *0.2-mm isotropic LSA imaging for around 10 min using CS TOF at 7T is feasible.*
● *More stems and branches of LSAs with longer lengths can be delineated with CS TOF than with conventional TOF at the same scan time.*
● *High-resolution CS TOF can be a promising tool for research and applications on LSA.*

Keywords MRI angiography · Magnetic resonance imaging · Lenticulostriate vasculopathy · Intracranial atherosclerosis · Cerebrovascular diseases

---

Z. Zhang and Q. Kong contributed equally to this article.

✉ Jing Jing
   jingj_bjttyy@163.com

1   Tiantan Neuroimaging Center of Excellence, Beijing Tiantan Hospital, Capital Medical University, No 119, South 4th Ring West Road, Fengtai District, Beijing 100070, China

2   China National Clinical Research Center for Neurological Diseases, Beijing, China

3   MR Collaboration, Siemens Healthineers Ltd., Beijing, China

4   Department of Neurology, Beijing Tiantan Hospital, Capital Medical University, Beijing, China

5   Siemens Healthcare GmbH, Erlangen, Germany

6   State Key Laboratory of Brain and Cognitive Science, Institute of Biophysics, Chinese Academy of Sciences, Beijing, China

7   University of Chinese Academy of Sciences, Beijing, China

Abbreviation

3D	Three-dimensional
7T	7 Tesla
ACA	Anterior cerebral artery
CS	Compressed sensing
DSA	Digital subtraction angiography
GRAPPA	Generalized autocalibrating partially parallel acquisitions
ICA	Internal carotid artery
LSA	Lenticulostriate artery
MCA	Middle cerebral artery
MIP	Maximum intensity projection
MOTSA	Multiple overlapping thin slab acquisition
MRI	Magnetic resonance imaging
MRA	Magnetic resonance angiography
SAR	Specific absorption rate
SNR	Signal-to-noise ratio
TOF	Time-of-flight
UHF	Ultra-high field

Introduction

Perforating arteries are small branches of the main cerebral arteries which supply the paramedian region of the brain stem, diencephalon, and central part of the cerebral hemispheres [1, 2]. Perforating arterial diseases, such as lipohyalinosis or fibrinoid necrosis of small perforating arteries and large-artery atherothromboses, which block the orifice of the small perforating arteries, could lead to lacunar infarctions that comprise approximately 25% of ischemic strokes [3]. An example of perforating arteries are the lenticulostriate arteries (LSAs), which branch from the middle cerebral artery (MCA), anterior cerebral artery (ACA), and the bifurcation of the internal carotid artery (ICA) [2, 4]. Understanding the artery characteristics that can describe the etiology or pathogenesis of LSA disease is an essential prerequisite for studying and treating lacunar infarction. However, the lack of reliable LSA imaging methods hinders related applications and research.

Currently, digital subtraction angiography (DSA) has been shown to be capable of imaging these vessels and is regarded as the "gold standard" in clinic practice; however, it is an invasive procedure given the need for an intra-arterial approach (i.e., arterial catheterization). 7T time-of-flight (TOF) magnetic resonance angiography (MRA) is an emerging non-invasive method to visualize LSAs, due to the increased signal-to-noise ratios (SNRs) and improved contrast at ultra-high fields (UHF) [4–7]. 7T TOF MRA enables the quantification of the number and length of LSA branches, and the metrics are found to be associated with disease symptoms [8–11]. However, high-resolution TOF MRA requires long acquisition times. Kang et al reported

LSA imaging with a voxel size of $0.23 \times 0.23 \times 0.36$ mm^3 in 10 min 27 s [4]. Mattern et al demonstrated an isotropic resolution of 0.15 mm with novel motion correction strategies in about 2 h [12]. We also managed to achieve 0.3-mm isotropic LSA imaging in 10 min 16 s using parallel imaging acceleration (GRAPPA = 3) [13] and partial Fourier acquisition. Thus, it can be challenging for conventional TOF MRA to achieve extremely high resolutions (e.g., $\leq$ 0.20 mm isotropic) within a patient's comfort and tolerance accommodated scan time (e.g., about 10 min), which hinders the large-scale clinical applications. Furthermore, the conventional acquisition with thin slab thickness using single-slab TOF MRA could result in insufficient coverage of the complete LSA vascular tree or over-saturated vessel signals [14], resulting in suboptimal MRA image quality.

It was recently demonstrated that the novel compressed sensing (CS) acceleration technique could be implemented in TOF MRA at 7T while preserving image quality [15–17]. Given its bright-blood nature, angiogram images are sparse in pixel representation, making CS suitable for MRA applications. Together with the improved signal and contrast of ultra-high fields, the acceleration potential of CS enables higher TOF MRA resolution at 7T. However, imaging protocols from previous studies might not be optimal for LSA extremely high-resolution imaging, since most of them focused on imaging over larger arterial territories or with reduced acquisition time [16, 17].

In this study, the imaging protocol was optimized for LSA coverage, and achieved 0.2-mm isotropic LSA imaging using CS TOF MRA, without significantly increasing the acquisition time. Specifically, the multiple overlapping thin slab acquisition (MOTSA) technique was used for less signal saturation [14, 18], and the segmented TOF scheme was used for the specific absorption rate (SAR) consideration at UHF [19]. The LSA images from CS TOF MRA were compared with optimized conventional 0.3-mm isotropic TOF MRA at the same scan time in healthy volunteers, in terms of LSA delineation (stem and branch numbers) and characterization (length and distance). Additionally, the delineation of LSAs using UHF CS TOF MRA was also compared with DSA in a patient with intracranial atherosclerosis.

Methods

Subjects

The initial technical evaluation was performed on seven healthy volunteers (aged 24–32 years, 2 males) prior to the study. The study recruited thirty healthy volunteers (aged 22–60 years, 10 males). All the healthy volunteers provided written informed consent for the in vivo experiments. For

direct comparison of LSA MRA with DSA, we studied one patient (42-year-old male, provided written informed consent) with symptomatic intracranial arterial stenosis on the M1 segment of the right MCA according to both DSA and 7T MRA.

All study was carried out in accordance with the institutional guidelines and with approval from the Ethics Committee of Beijing Tiantan Hospital.

MRI data acquisition

All MR scans were performed on a 7-T MR system (MAGNETOM Terra, Siemens Healthcare) using a 32-channel Rx/8Tx head-coil (Nova Medical) with a circular polarized B1 mode.

An optimized 0.3-mm isotropic conventional TOF MRA was performed. Compared with previous work [4, 11], the optimization included increasing the flip angle, adopting multi-slab scans, and achieving local shimming. The imaging parameters for conventional TOF MRA included an oblique axial orientation, MOTSA [18] slabs = 4, slab thickness = 13.2 mm, field of view = $202 \times 179 \times 42.9$ mm^3, voxel size = $0.3 \times 0.3 \times 0.3$ mm^3, TR/TE = 15/5.61 ms, flip angle = 23°, GRAPPA acceleration = 3, no venous suppression, and acquisition time = 10 min 16 s.

A prototype CS TOF MRA was used to achieve 0.2-mm isotropic LSA imaging. The imaging parameters included oblique axial orientation, MOTSA slabs = 4, slab thickness = 12.6 mm, field of view = $196 \times 172 \times 42.8$ mm^3, voxel size = $0.2 \times 0.2 \times 0.2$ mm^3, TR/TE = 15/5.61 ms, flip angle = 23°, CS acceleration = 8 (effective acceleration = 7.2), sparse venous saturation with segmentation = 4, and acquisition time = 10 min 14 s. The CS reconstruction was performed on a scanner following the previous study [17].

In addition, for the initial technical evaluation, an additional 0.2-mm convention TOF (acquisition time = 19 min 38 s) and 0.3-mm CS TOF (acquisition time = 5 min 33 s) were also performed in the seven volunteers prior to the study. The parameters were the same except for the acquisition voxel size.

Both CS TOF and conventional TOF MRA were used to image LSAs and MCAs, and the shimming area was adjusted to cover only the LSA area before scanning. Before imaging the target vessels with high resolution, a scout TOF-MRA with isotropic 1-mm voxel size and 70-mm axial coverage was applied as a vessel localizer.

DSA data acquisition

Compared with the 7T CS TOF MRA study, conventional cerebral angiographic examinations were performed using a biplane angiographic unit (Axiom Artis dTA, Siemens Medical Systems) using transfemoral catheterization. Iodinated contrast material (iopromide, Ultravist 300 mg/L Bayer Schering Pharma AG) was administrated with a power injector through a 5-F catheter. The examination consisted of a four-vessel 2D-DSA and 3D-DSA of the artery. The 3D-DSA imaging was based on rotational acquisitions, covering 200°, resulting in 395 two-dimensional source images in cine mode. The contrast agent was administered at a volume of 24 mL (6 mL/s) to carotid arteries and 18 mL (3 mL/s) to vertebral arteries.

Data analysis

The initial technical evaluation and the cohort experiment followed the same process as below. Images were reviewed and analyzed using commercial software (OsiriX MD, Pixmeo SARL). Healthy subjects with either CS or conventional TOF images corrupted by motion artifacts were excluded from the analysis. Both TOF MRA images were reformatted into coronal planes, and consecutive maximum intensity projections (MIPs) with a 20-mm thin slab were created. Using the coronal reformatted and raw images, the LSAs arising from the M1 segment of the MCA, ACA, and bifurcation of ICA were visually identified and then evaluated as follows. The most prominent branch of the LSAs was identified in each hemisphere.

For the image quality evaluation, the contrast-to-noise ratio (CNR) and contrast ratio (CR) were calculated at 5 mm above the MCA M1 between the prominent LSA and surrounding brain tissue. The ROI areas for CNR and CR measurements were set in a circle around 0.8 mm^2. The CNR was defined as follows: CNR = (mean (Signal$_{LSA}$) − mean (Signal$_{tissue}$)) / std (Noise). The CR was defined as follows: CR = (mean (Signal$_{LSA}$) − mean (Signal$_{tissue}$)) / mean (Signal$_{tissue}$). The SNR was calculated at two locations that are MCA M1 (SNR$_{mca}$) and brain tissue (SNR$_{tissue}$). The ROI areas for SNR measurements were set in a circle around 3 mm^2. The noise was measured at regions with no anatomical structures. All the above signal measurements were performed on the raw images. Detailed methods have been described in previous work [11].

For the LSA delineation and characterization, SimVascular software (http://simvascular.github.io/) [20] was used to build the vascular skeleton by manually tracing the center lines of the MCAs and LSAs. This open-source software package allows for the modeling and segmentation of vasculature, and has been used in numerous cardiovascular and neurovascular studies [11, 21]. Tracing was manually performed by a neuroscientist (Q.L.K., with 5 years of experience in MRI image interpretation) who was blinded to the data and recursively screened the raw TOF images and delineated the center points along each visible arterial segment. Tracing continued as long as the contrast ratio (CR) between the LSA lumen and adjacent tissue was above 1.1. The generated 3D skeletons of LSAs were examined by a

neuroscientist and a senior neurologist (Z.Z., J.J.; 8 and 15 years of experience in TOF MRA, respectively), ensuring that the skeletons reflected the central lines of the LSAs, and the delineated length was reasonable according to the pre-defined CR criterion. Cases with disagreement were reviewed together and resolved by consensus. The number of stems, number of branches, total length, and distance between the origin and terminal point were analyzed on the skeletonized vascular tree. Stems were defined as LSAs that originated directly from the MCA M1, and branches were defined as daughter vessels originating from the parent LSA stems plus stem without any branches [9]. The total length and distance were measured from the most prominent LSA in each hemisphere.

Statistical analysis

All quantitative data were expressed as means ± standard deviations. The Wilcoxon signed-rank test was used to compare the numbers of stems and branches between the two imaging methods. A p-value < 0.05 indicated statistical significance. The lengths and distances of the most prominent LSA branch acquired by CS TOF MRA and conventional TOF MRA were compared using Bland-Altman plotting and a paired-sample t-test. Intraclass correlation coefficient (ICC) was calculated and reported for all morphologic LSA measurements. All statistical analyses were performed using commercial software (SPSS 22.0, IBM).

Results

For the initial technical evaluation, the representative coronal LSA MIPs for the four scans (0.2-mm conventional and CS TOF, 0.3-mm conventional and CS TOF) are shown in Supplementary Fig. 1. Totally, 4 out of 7 healthy volunteers obtained 0.2-mm conventional TOF images with acceptable quality, which results from the motion artifact and arterial pulsation artifacts. All 7 volunteers obtained acceptable quality 0.2-mm CS TOF, 0.3-mm conventional TOF, and 0.3-mm CS TOF images. The SNR and CNR for the four scans (0.2-mm conventional and CS TOF, 0.3-mm conventional and CS TOF) are summarized in Supplementary Table 1. For all 4 volunteers, the 0.3-mm CS TOF had the highest SNR, followed by the 0.3-mm conventional TOF, and then the 0.2-mm CS TOF, with the 0.2-mm conventional TOF having the lowest SNR. For the CNR evaluation, the 0.3-mm CS TOF has the highest CNR, the 0.2-mm conventional TOF has the lowest CNR, but the 0.2-mm CS TOF has a higher CNR than the 0.3-mm conventional TOF.

Fifty-two hemispheres from twenty-six healthy volunteers were included in the analysis with the acceptable image quality from both CS TOF and conventional TOF. The representative axial images and coronal MIPs from CS TOF and conventional TOF in a healthy volunteer are shown in Fig. 1. Small arteries were observed in both CS raw and MIP images (red arrows, Fig. 1).

Fig. 1 Comparison of conventional TOF images and CS TOF images in axils section (top row) and coronal MIPs (slab thickness = 20 mm, bottom row). CS TOF images show more LSAs (red arrows). CS, compressed sensing; LSAs, lenticulostriate arteries; MIPs, maximum intensity projections; TOF, time-of-flight
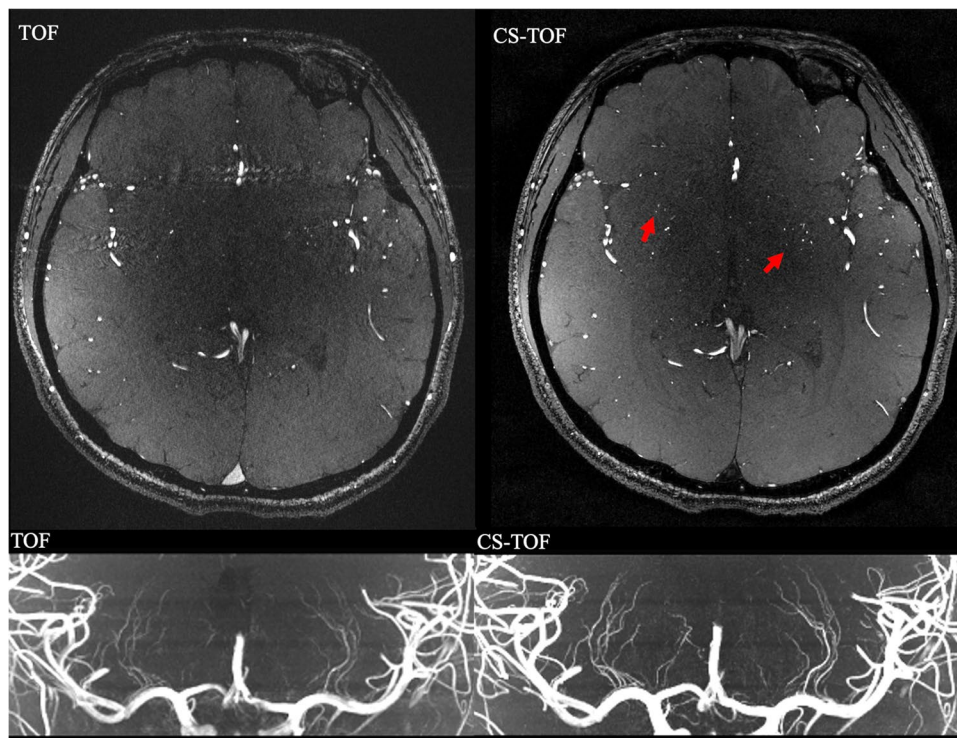
The representative MIPs, as well as traced vessel skeletons generated from another volunteer, are demonstrated in Fig. 2. In general, the traced vessel skeletons of both methods demonstrated identical basic structures (Fig. 2). However, in almost all instances, CS TOF MRA showed more LSA branches in visual inspections (identical to the following quantitative evaluation, in Table 1).

The SNRs measured at two positions for the two methods are illustrated in Supplementary Figs. 2a and 2b. The SNRs in CS TOF were significantly lower than TOF at both two positions for all hemispheres (SNR_{mca}, left: $p = 0.002$, right: $p = 0.012$; SNR_{tissue}, left: $p < 0.001$, right: $p < 0.001$). The lumen-tissue CNRs measured with the two methods are illustrated in Supplementary Fig. 2c. CS TOF yielded CNR lightly higher than conventional TOF, but there is no significant difference. Supplementary Fig. 2d shows CS TOF has a higher contrast ratio in all hemispheres (left: 4.7 ± 1.6 vs. 2.7 ± 0.8, $p < 0.001$; right: 4.4 ± 1.2 vs. 2.5 ± 0.8, $p < 0.001$).

The numbers of LSA stems and branches are summarized in Table 1. The number of stems visualized on CS TOF was significantly higher than on conventional TOF (left: 7.4 ± 1.7 vs. 6.8 ± 1.6, $p = 0.002$, ICC $= 0.884$; right: 7.7 ± 1.8 vs. 6.9 ± 1.9, $p < 0.001$, ICC $= 0.938$). The number of branches visualized by conventional TOF was significantly lower than that by CS TOF MRA (left: 24.0 ± 5.1 vs. 17.8 ± 4.3, $p < 0.001$, ICC $= 0.893$; right: 25.3 ± 5.8 vs. 18.2 ± 4.5, $p < 0.001$, ICC $= 0.896$) (Fig. 3).

Lengths were statistically higher in CS TOF than in conventional TOF (left: 55.4 ± 4.2 vs. 51.3 ± 5.0, $p < 0.001$, ICC $= 0.868$; right: 55.5 ± 4.4 vs. 51.1 ± 4.5, $p < 0.001$, ICC $= 0.876$). The distance was also statistically higher in CS TOF than in conventional TOF (left: 42.6 ± 4.6 vs. 39.5 ± 5.1, $p < 0.001$, ICC $= 0.916$; right: 40.7 ± 3.6 vs. 37.8 ± 3.9, $p < 0.001$, ICC $= 0.913$). This result demonstrated that the vasculature visible using CS TOF was significantly longer than that of conventional TOF (Fig. 4).

For the patient with intracranial atherosclerosis, the 2D DSA showed limited delineation of LSAs, especially for branches, whereas CS TOF delineates clear outlines and origins of LSAs, and the distal branches (Fig. 5). Although 3D DSA has a better delineation of LSAs than 2D DSA, the visual depiction of distal LSA branches is still inferior to that of CS TOF (red arrows, Fig. 5).

Discussion

Using the 7T CS TOF technique, detailed in vivo MRA of LSAs at 0.2-mm isotropic resolution was obtained. This study compared the LSA numbers of stems, branches, length, and distance between CS TOF and conventional TOF. Results show that more stems and branches with longer lengths can be delineated with CS TOF than with conventional TOF, suggesting CS TOF MRA at 7T can be a promising technique for characterizing LSA.

LSAs primarily feed the corpus striatum in the sub-cortex and are essential for ensuring blood supply to the brain. Assessment of LSA patency may provide crucial information on risk stratification and treatment response. However, it can be difficult to determine the pathogenesis of LSA-territorial infarcts mainly because conventional imaging modalities (3 T MRI/MRA, CTA) have been incapable of properly visualizing with LSAs and their abnormalities. Recently, ultrahigh-field magnetic resonance scanners have become available, and high-resolution imaging at 7T has been applied for the direct assessment of perforating arteries using MRA.

For the potential of visualizing more LSAs, one 7T study [9] has shown fewer numbers of stems and branches

Fig. 2 The CS TOF and conventional TOF MIPs of one volunteer (slab thickness = 20 mm) and corresponding vascular skeletons. The extracted vascular trees show more branches in CS TOF-MRA than in conventional TOF. CS, compressed sensing; MRA, magnetic resonance angiography; MIP, maximum intensity projection; TOF, time-of-flight
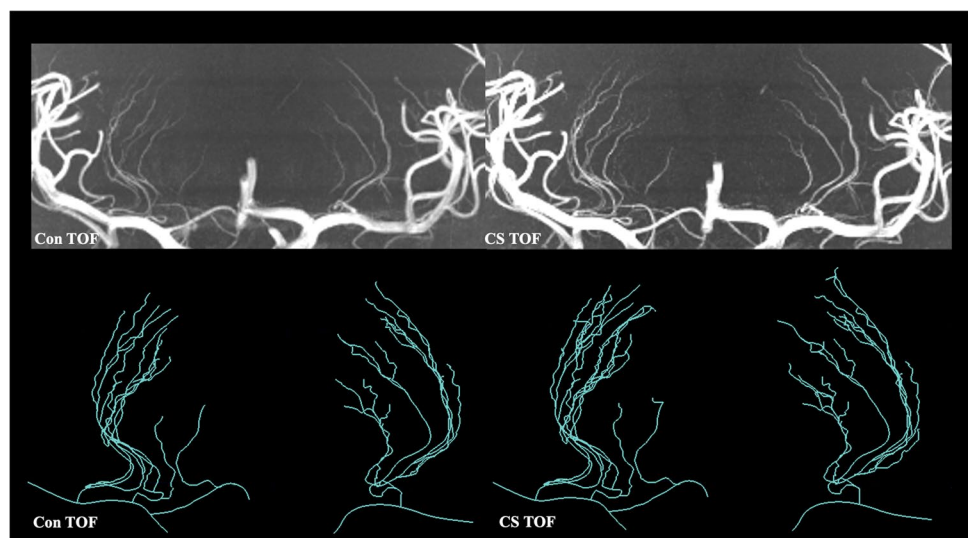
Table 1 Numbers of LSA stems and branches visualized by CS TOF and conventional TOF at 7T, in the left and right hemispheres

Subject	Left hemisphere				Right hemisphere			
	Stems		Branches		Stems		Branches	
	CS-TOF	TOF	CS-TOF	TOF	CS-TOF	TOF	CS-TOF	TOF
S01	5	4	22	12	10	9	30	22
S02	6	5	20	17	9	8	26	17
S03	7	6	25	22	7	6	26	20
S04	5	5	20	15	7	6	24	17
S05	7	5	22	16	6	6	30	23
S06	9	7	17	13	8	8	16	11
S07	5	4	17	11	8	7	18	11
S08	5	5	21	18	7	6	29	21
S09	9	8	24	18	8	7	22	17
S10	9	8	26	22	9	8	32	21
S11	6	6	23	14	6	5	18	13
S12	6	6	17	13	6	4	21	12
S13	7	7	25	17	7	7	30	21
S14	9	8	23	17	5	5	25	18
S15	7	6	19	15	8	6	24	15
S16	8	8	34	27	12	12	34	25
S17	9	9	32	23	10	9	29	22
S18	9	9	35	26	6	6	23	17
S19	6	6	31	22	7	6	24	17
S20	9	9	26	19	11	11	30	25
S21	5	5	24	20	4	4	17	13
S22	9	7	24	16	7	6	26	15
S23	8	7	18	14	6	6	17	14
S24	8	8	26	18	9	7	30	22
S25	11	9	22	15	8	7	19	17
S26	8	9	30	24	8	7	38	27

in hypertensive patients than healthy subjects. Another 7T study [8] reported fewer lenticulostriate arteries supplying the region of the basal ganglia in stroke patients compared to healthy controls. Besides the number of LSAs, studies have also reported morphology-related characteristics, for example, higher curvature and tortuosity in hypertensive patients [9] and shorter length and distance in symptomatic side infarction patients. These and several other studies [10, 22, 23] using 7T high-resolution MRA have revealed that the visualization, numbers, and morphology-related characteristics of LSAs help to illustrate the pathogenesis of stroke and cardiovascular disease–related characteristics.

Ex vivo anatomy studies suggested that the number of LSAs was significant and ranged in diameter from 0.08 to 1.5 mm [24]. Currently, most 7T TOF MRA imaging resolutions are around 0.3 mm, and increasing the resolution to 0.2 mm may cover more spectrum of the lenticulostriate artery ranges. Theoretically, higher resolution may allow more lenticulostriate arteries to be visualized, but the higher resolution (> 0.2 mm) may require a longer scan time (may result in a low imaging success rate). A previous study reported more than a 2-h scan for 0.15 mm MRA [12]. Considering the previous 7T TOF MRA studies on the lenticulostriate artery scan [7, 19, 25, 26] and our 7T experience, we designed to achieve 0.2 mm of around a 10-min scan for LSA MRA to balance image quality (for quantification) and subject comfort (less possibility of motion-related artifact, since our 20-min scans have a success rate of 4/7). The compressed sensing technique applied has been demonstrated to improve the SNR efficiency while preserving imaging quality due to its novel acquisition trajectory (2D undersampling pattern with about eightfold acceleration) and reconstruction [16, 17], and signal sparsity nature of MRA. This initial study suggested that 10-min CS TOF with a 0.2-mm resolution can currently be one of the reliable and applicable methods for LSA high-resolution imaging. With the next-generation imaging acceleration techniques such as deep learning [27], TOF MRA may be further improved for better LSA visualization and characterization.
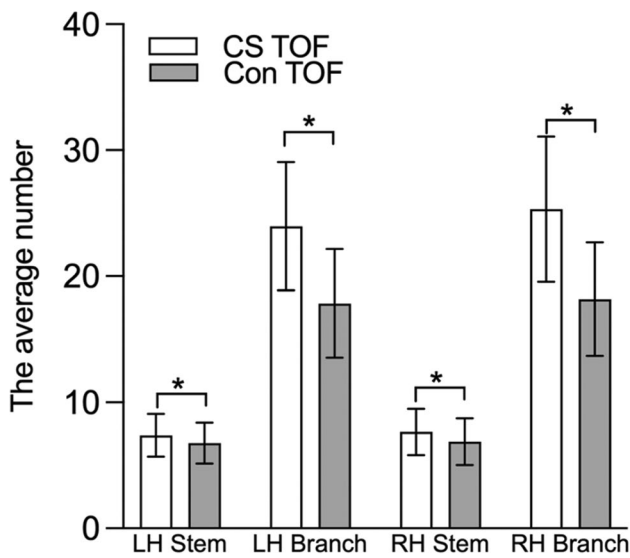
Fig. 3 Stems and branches of LSAs visualized by CS TOF-MRA and conventional TOF-MRA (Con TOF). *Statistically significant difference. CS, compressed sensing; LSA, lenticulostriate artery; MRA, magnetic resonance angiography; TOF, time-of-flight

Compared with previous MRA studies [4, 11], more stems, branches, and longer lengths of LSAs were reported in this study, for both CS TOF and conventional TOF. This can be due to optimized acquisition parameters and different artery inclusion criteria: the longer TR/larger flip angle (for reducing the saturation of slow-flowing blood) and the MOTSA technique (instead of one slab acquisition for reducing avoid venetian blind artifacts) [4, 11, 18]. Four slabs with 18.6% oversampling were used in this study to cover all LSA regions. Further optimizations of the sequence can be explored such as a lower resolution in the z-direction for better SNR efficiency. Different artery inclusion criteria were employed in the evaluation. All LSAs were counted, including LSAs from the M1 segment of the MCA, ACA, and bifurcation of ICA, whereas Zhang et al only counted LSAs that originated from MCA M1 [11]. Also different post-processing methods were adopted. This study managed to avoid fainted distal end contrast problems using manually tracing the vascular skeleton on raw images instead of counting the LSA numbers based on conventional 2D MIP images [4]. These optimizations in acquisition and processing enable TOF for better LSA characterization, even on the conventional TOF images in the study.

DSA is commonly considered the "gold standard" for LSA visualization. Kang et al suggested that the distribution

Fig. 4 Bland-Altman plots represent the differences in (**a**) lengths and (**b**) distance measured in the predominant vascular trees of CS TOF and TOF in the right and left hemispheres (RH/LH). CS TOF shows longer LSA vasculature in both length and distance. CS, compressed sensing; LSA, lenticulostriate artery; TOF, time-of-flight
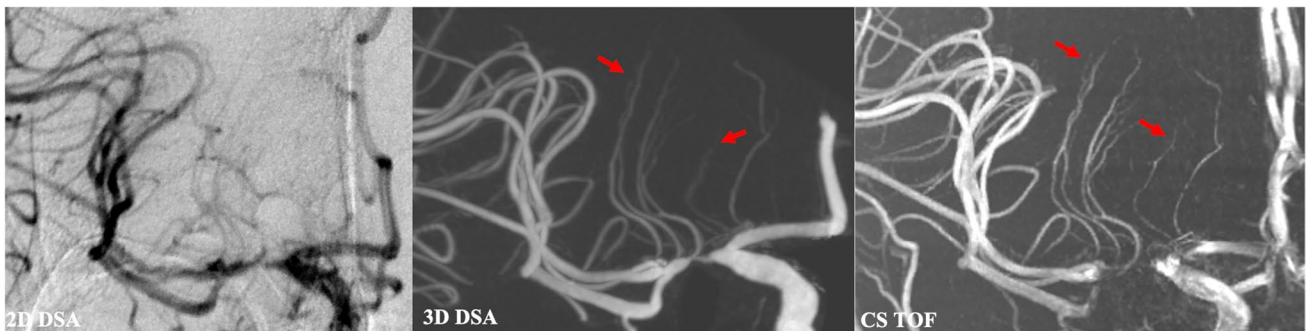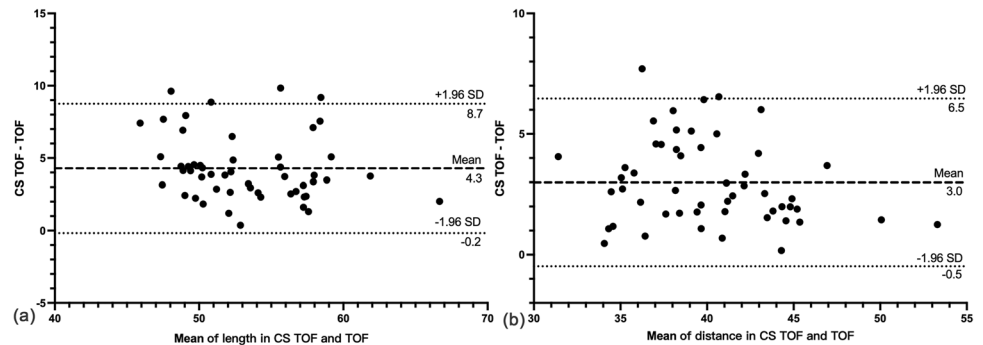

Fig. 5 Comparisons of LSA between CS TOF and DSA in a patient with symptomatic intracranial arterial stenosis on M1 segment of right MCA. Both DSA images (2D and 3D) showed inferior visual delineation of LSAs compared with CS TOF. CS, compressed sensing; DSA, digital subtraction angiography; LSA, lenticulostriate artery; MCA, middle cerebral artery; TOF, time-of-flight

of LSAs can be visualized by DSA with a 3D reconstruction of rotational angiography [28]. Our initial results showed that CS TOF has better outlines and delineations of LSA branches (Fig. 5) compared with both 2D and 3D DSA. In addition, it is challenging to track LSA branches on routine 2D DSA due to the faint filling of LSA branches and the disturbance of other vascular branches. Moreover, DSA is invasive and requires intra-arterial catheterization, which may carry substantial risks of morbidity or mortality [29]. Thus, the DSA technique might not be the method of choice for screening healthy individuals or asymptomatic patients if the subject appears to have risk factors for stroke. Whether CS TOF can replace DSA and become the gold standard of LSA imaging needs to be further verified in more settings.

There are several limitations in our study. Firstly, the reconstruction of CS TOF is time-consuming (~ 12 min) compared with conventional parallel imaging reconstruction (instant results after acquisition). The reconstruction time is nearly the same as the acquisition time for CS TOF and will take longer with an increased acquisition matrix or the number of slabs. The reconstruction time can be addressed with better hardware and new reconstruction approaches. Secondly, the vessel manual tracing method was implemented in the research. While it can be precise for LSA delineations for this pilot research, the time-consuming labeling, which takes hours to complete, may also hinder the clinical applications. Advanced automatic tracing, segmentation, reconstruction, and analysis of LSAs should be introduced to facilitate fast and objective characterizations of arterioles. Thirdly, the SNR/CNR measurements did not consider the effect of parallel imaging or compressed sensing for noise distribution. Lastly, this preliminary study included a relatively small number of samples. The fidelity of using 7T CS TOF for imaging LSAs and the clinical impact of LSA findings should be evaluated further in a larger population and patients.

Conclusions

This work demonstrates the feasibility of 0.2-mm LSA imaging using CS TOF MRA. A higher resolution produces detailed delineation and better characterization of the LSAs. The clinical value of CS TOF at 7T for imaging LSAs should be evaluated in populations with different neurologic diseases.

Declarations

References

1. Ghika JA, Bogousslavsky J, Regli F (1990) Deep perforators from the carotid system: template of the vascular territories. Arch Neurol 47:1097–1100. https://doi.org/10.1001/archneur.1990.00530 100063014

2. Djulejić V, Marinković S, Milić V et al (2015) Common features of the cerebral perforating arteries and their clinical significance. Acta Neurochir (Wien) 157:743–754. https://doi.org/10.1007/s00701-015-2378-8

3. Hart RG, Diener H-C, Coutts SB et al (2014) Embolic strokes of undetermined source: the case for a new clinical construct. Lancet Neurol 13:429–438. https://doi.org/10.1016/S1474-4422(13)70310-7

4. Kang C-K, Park C-W, Han J-Y et al (2009) Imaging and analysis of lenticulostriate arteries using 7.0-Tesla magnetic resonance angiography. Magn Reson Med 61:136–144. https://doi.org/10.1002/mrm.21786

5. Cho Z-H, Kang C-K, Han J-Y et al (2008) Observation of the lenticulostriate arteries in the human brain in vivo using 7.0T MR angiography. Stroke 39:1604–1606. https://doi.org/10.1161/STROKEAHA.107.508002

6. Kong Q, Zhang Z, Yang Q et al (2019) 7T TOF-MRA shows modulated orifices of lenticulostriate arteries associated with atherosclerotic plaques in patients with lacunar infarcts. Eur J Radiol 118:271–276. https://doi.org/10.1016/j.ejrad.2019.07.032

7. von Morze C, Xu D, Purcell DD et al (2007) Intracranial time-of-flight MR angiography at 7T with comparison to 3T. J Magn Reson Imaging 26:900–904. https://doi.org/10.1002/jmri.21097

8. Kang C-K, Park C-A, Park C-W et al (2010) Lenticulostriate arteries in chronic stroke patients visualised by 7 T magnetic resonance

angiography. Int J Stroke 5:374–380. https://doi.org/10.1111/j.1747-4949.2010.00464.x

9. Kang C-K, Park C-A, Lee H et al (2009) Hypertension correlates with lenticulostriate arteries visualized by 7T magnetic resonance angiography. Hypertension 54:1050–1056. https://doi.org/10.1161/HYPERTENSIONAHA.109.140350

10. Seo SW, Kang C-K, Kim SH et al (2012) Measurements of lenticulostriate arteries using 7T MRI: new imaging markers for subcortical vascular dementia. J Neurol Sci 322:200–205. https://doi.org/10.1016/j.jns.2012.05.032

11. Zhang Z, Fan Z, Kong Q et al (2019) Visualization of the lenticulostriate arteries at 3T using black-blood T1-weighted intracranial vessel wall imaging: comparison with 7T TOF-MRA. Eur Radiol 29:1452–1459. https://doi.org/10.1007/s00330-018-5701-y

12. Mattern H, Sciarra A, Godenschweger F et al (2018) Prospective motion correction enables highest resolution time-of-flight angiography at 7T: prospectively motion-corrected TOF angiography at 7T. Magn Reson Med 80:248–258. https://doi.org/10.1002/mrm.27033

13. Griswold MA, Jakob PM, Heidemann RM et al (2002) Generalized autocalibrating partially parallel acquisitions (GRAPPA). Magn Reson Med 47:1202–1210. https://doi.org/10.1002/mrm.10171

14. Blatter DD, Parker DL, Robison RO (1991) Cerebral MR angiography with multiple overlapping thin slab acquisition. Part I. Quantitative analysis of vessel visibility. Radiology 179:805–811. https://doi.org/10.1148/radiology.179.3.2027996

15. Lustig M, Donoho D, Pauly JM (2007) Sparse MRI: the application of compressed sensing for rapid MR imaging. Magn Reson Med 58:1182–1195. https://doi.org/10.1002/mrm.21391

16. Park C-A, Kang D, Son Y-D et al (2015) Microvascular imaging using compressed sensing at 7T MRI: a preliminary study. Appl Magn Reson 46:1189–1197. https://doi.org/10.1007/s00723-015-0713-0

17. Meixner CR, Liebig P, Speier P et al (2019) High resolution time-of-flight MR-angiography at 7 T exploiting VERSE saturation, compressed sensing and segmentation. Magn Reson Imaging 63:193–204. https://doi.org/10.1016/j.mri.2019.08.014

18. Parker DL, Yuan C, Blatter DD (1991) MR angiography by multiple thin slab 3D acquisition. Magn Reson Med 17:434–451. https://doi.org/10.1002/mrm.1910170215

19. Zhang Z, Deng X, Weng D et al (2015) Segmented TOF at 7 T MRI: technique and clinical applications. Magn Reson Imaging 33:1043–1050. https://doi.org/10.1016/j.mri.2015.07.002

20. Updegrove A, Wilson NM, Merkow J et al (2017) SimVascular: an open source pipeline for cardiovascular simulation. Ann Biomed Eng 45:525–541. https://doi.org/10.1007/s10439-016-1762-8

21. Sengupta D, Kahn AM, Burns JC et al (2012) Image-based modeling of hemodynamics in coronary artery aneurysms caused by Kawasaki disease. Biomech Model Mechanobiol 11:915–932. https://doi.org/10.1007/s10237-011-0361-8

22. Miyazawa H, Natori T, Kameda H et al (2019) Detecting lenticulostriate artery lesions in patients with acute ischemic stroke using high-resolution MRA at 7 T. Int J Stroke 14:290–297. https://doi.org/10.1177/1747493018806163

23. Ling C, Fang X, Kong Q et al (2019) Lenticulostriate arteries and basal ganglia changes in cerebral autosomal dominant arteriopathy with subcortical infarcts and leukoencephalopathy, a high-field MRI study. Front Neurol 10:870. https://doi.org/10.3389/fneur.2019.00870

24. Vogels V, Dammers R, van Bilsen M et al (2021) Deep cerebral perforators: anatomical distribution and clinical symptoms: an overview. Stroke 52(10):e660–e674. https://doi.org/10.1161/STROKEAHA.120.034096

25. Harteveld AA, De Cocker LJL, Dieleman N et al (2015) High-resolution postcontrast time-of-flight MR angiography of intracranial perforators at 7.0 Tesla. PLoS One 10:e0121051. https://doi.org/10.1371/journal.pone.0121051

26. Liem MK, van der Grond J, Versluis MJ et al (2010) Lenticulostriate arterial lumina are normal in cerebral autosomal-dominant arteriopathy with subcortical infarcts and leukoencephalopathy: a high-field in vivo MRI study. Stroke 41:2812–2816. https://doi.org/10.1161/STROKEAHA.110.586883

27. Muckley MJ, Riemenschneider B, Radmanesh A et al (2021) Results of the 2020 fastMRI challenge for machine learning MR image reconstruction. IEEE Trans Med Imaging 40:2306–2317. https://doi.org/10.1109/TMI.2021.3075856

28. Kang H-S, Han MH, Kwon BJ et al (2005) Evaluation of the lenticulostriate arteries with rotational angiography and 3D reconstruction. AJNR Am J Neuroradiol 26(2):306–312

29. Cloft HJ, Joseph GJ, Dion JE (1999) Risk of cerebral angiography in patients with subarachnoid hemorrhage, cerebral aneurysm, and arteriovenous malformation: a meta-analysis. Stroke 30:317–320. https://doi.org/10.1161/01.STR.30.2.317